A Hierarchical Machine Learning Model to Predict the Modulus of Bi-Soft Segment Polyurethanes

Calvin Gang, Joseph Pugar, Newell Washburn

Carnegie Mellon University

March 1, 2022

Abstract

Thermoplastic polyurethanes (TPU) are linear segmented block copolymers that can access a wide range of properties by leveraging the formation of hard and soft phase-segregated microdomains. One method to tune TPU properties is to synthesize bi-soft segment TPU (biSS-TPU), which combine two polyol components in the soft phase such that their polar incompatibility can influence behavior at the hard-soft phase interface. This work proposes a method for training a hierarchical machine learning model to predict biSS-TPU modulus values. A random forest is demonstrated to have accurate predictions over multiple random train-test splits, and three of the most significant predictors were identified by a combined recursive feature elimination and permutation importance method. To achieve high accuracy, the model learned to determine the presence and magnitude of mixing effects, defined as non-linear changes to the modulus due to the thermodynamic incompatibility of two soft segment components.

Introduction

Thermoplastic polyurethanes (TPU) are ubiquitous materials found in applications including coatings, foams, elastomers, and biomedical devices.[1] When prepared as segmented block copolymers, TPU's undergo a phase segregation process, in which chain segments consisting of diisocyanate and low molecular weight glycols aggregate into hard microdomains within a relatively mobile soft phase matrix.[2,3] Chain segments in the hard phase adopt an extended configuration, fortified by hydrogen bonding among urethane groups and crystallization of highly ordered interior regions. This gives the TPU a nanocomposite-like structure depicted in figure 1, except with covalently bonded hard and soft segments.

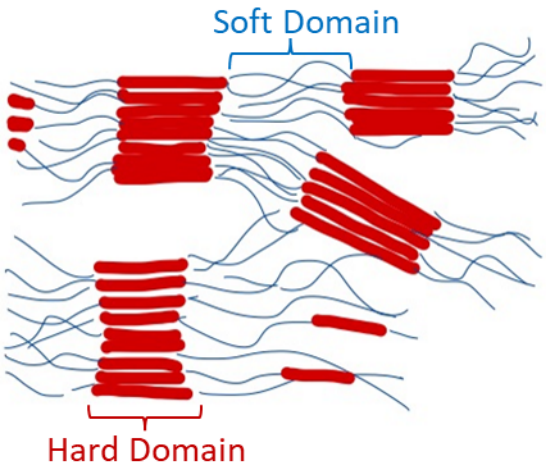

Figure 1. Schematic of a TPU microstructure

Although bi-soft segment TPU (biSS-TPU) have been seldom studied in literature, the niche material has contributed to a number of practical technologies, including shape-memory polymers[4] and thin film membranes.[5, 6, 7, 8] In some cases, the mixing of polyol components in a TPU soft phase have enhanced performance properties.[5, 9, 10] For instance, a biSS-TPU synthesized with polyethylene glycol (PEG) and polypropylene glycol (PPG) exhibited better thermal and electrochemical stability than single soft segment TPU (sSS-TPU) counterparts.[9]

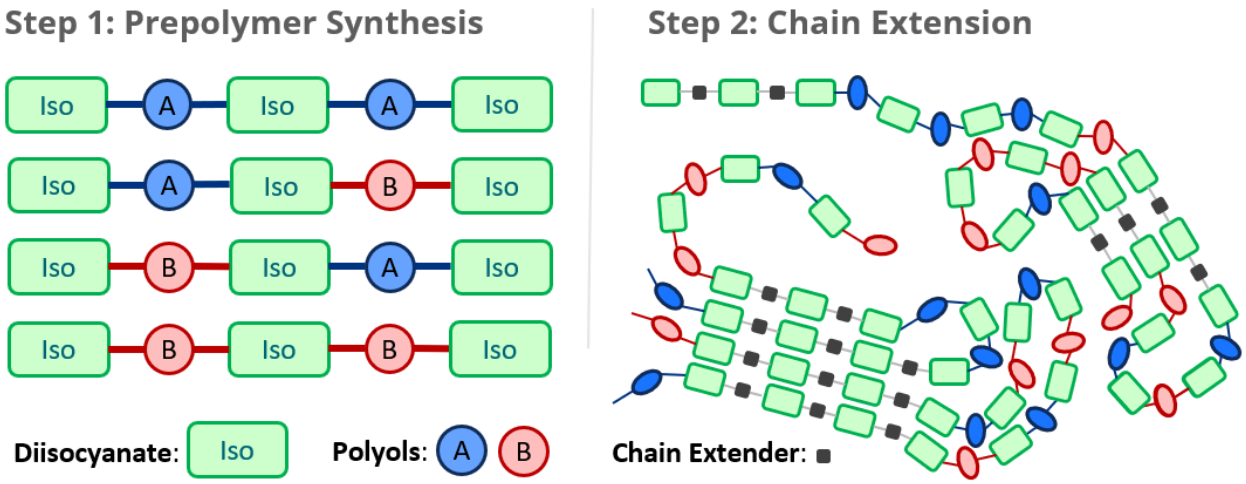

Figure 2. Schematic of a speculated biSS-TPU microstructure

One can consider biSS-TPU to be linear multiblock copolymers (LMBCP) with random Markovian sequences of either polyol A or B blocks linked together by hard segment units. Therefore, thermodynamics of the biSS phase can be understood by considering the theorical basis for the behavior of a two-phase block copolymer.[11] The elegance of BCP's is that they may form a single molecular chain consisting of two or more thermodynamically incompatible polymer blocks to drive segregation into distinct microphases.[12] In the case of a block copolymer which aggregates into a microdomain rich in A-type blocks and a separate B-type microdomain, the entropy of mixing per unit volume of dissimilar block segments is substantially smaller than that of small molecules.[13] Thus, minor chemical or structural differences between A and B blocks would drive the free energy to disfavor mixing if it were not for the covalent linkages between A and B blocks resisting macroscale separation. The resulting tension forces the backbone to adopt an entropically less favorable extended configuration.[12] Therefore, BCPs strike a balance between an entropic restoring force and thermodynamic monomer incompatibility to limit phase separation to the mesoscale (~10 nm).

Behavior at the A-B interface is often parameterized by phase composition (f, where f = 0.5 is equivalent to a 1:1 ratio of polyols A and B), degree of polymerization (DP), and the Flory-Huggins interaction parameter, χ.[16] Polymer chemists stake a particular interest in χ, because it reflects cost to free energy of the enthalpic contacts between monomer units.[15] Traditionally, χ takes on positive (disfavoring mixing) values less than unity, but inclusion of key

moieties in the monomer structure can open small windows of miscibility through specific interactions, such as hydrogen bonds.[17, 18, 19] χ is defined as follows:

$$\chi_{AB} = \left(\frac{Z}{k_B T}\right)\left[\varepsilon_{AB} - \frac{1}{2(\varepsilon_{AA} + \varepsilon_{BB})}\right]$$

Where Z is the number of nearest-neighbor monomer contacts, $k_B T$ is thermal energy, and ε_{ij} is the pairwise interaction between monomers i and j.

To understand biSS mixing effects, one must consider how the incompatibility of SS components ultimately influences the propensity of the hard and soft phases to segregate. Liu et al, provided the most direct characterization of biSS-TPU microphase separation to date. They used amplitude modulated-frequency modulated viscoelastic mode of atomic force microscopy (AM-AFM) to identify the spatial location of hard and soft domains in biSS-TPU.[8] In contrast to the dense, large and consistent sSS-TPU hard domains, biSS-TPU hard domains were predominantly dispersed in a mesophase of intermediate modulus domains attributed to randomly alternating A-B-HS units. Moreover, biSS mixing has been shown to disrupt hydrogen bonding within the hard domain via Fourier-Transform infrared spectroscopy (FTIR). X-ray diffraction at low angles of 2θ, suggested that biSS mixing reduced the crystallinity of hard phases as well. Thus, characterization of biSS-TPU microphase separation has formed a consensus that biSS mixing generally disperses the hard segment among soft segment units, such that macroscopic properties depend not only on the total hard segment content, but also on the size and distribution of hard domains.

Furthermore, the diisocyanate in biSS-TPU synthesis takes on an additional role of mediating miscibility of polyols in the soft phase to result in decreased H-S phase segregation.[14, 15, 16] The Liemenstoll group demonstrated that mixing effects, of the biSS-TPU originate from polar incompatibilities of polyol units in ternary oligomeric prepolymer mixtures. Using Van Krevelen and Stefanis group contribution estimates of solubility parameters, they estimated ternary phase diagrams by treating the diisocyanate as a solvent.[16] In another study, they synthesized isocyanate-terminated TPU oligomers from mixed polyols allowing for characterization of SS unit sequences to simulate reaction-induced phase separation in a TPU prepolymer.[15] Here, ^{1}H-NMR was used to monitor the conversion of hexamethylene diisocyanate (HDI) with an equimolar polyol mixture comprising primary and secondary hydroxyl-terminated

polyols (PPO_{2000} and PEO_{590}) at a 3:2 NCO:OH index. Competing end group kinetics resulted in random consecutive incorporation of different polyol types, forming a phase-separated blend of blocked oligomers. Understanding the mechanism of the reaction-induced phase separation of biSS-TPU prepolymers provided the foundation for interpreting how tensions originating from polar dissimilarities of blocks within the soft phase may influence the strength of separation at the hard-soft interface.

Recently, machine learning has become a powerful tool for the exploration of structure-property relationships of complex polymer material systems toward the accelerated design of high-performance polymers.[17, 18] At this time, the unbalanced and low experimental throughput of typical polymer laboratories poses a major challenge to the use of machine learning for polymer design. Polymer projects often encompass only dozens of experiments, as opposed to the thousands necessary for most machine learning algorithms. This project sought to train a machine learning model that can learn structure-property relationships of complex bi-SS TPU systems while limited to the typical experimental throughput of polymer laboratories. To demonstrate a proposed workflow, a model was fitted to learn mixing effects in order to predict biSS-TPU modulus, a fundamental measure of material stiffness.

Given the complexity of polymeric materials, spanning multiple length and time scales, many natural phenomena of polymers may be expected to require an intricate network of unobservable latent variables that map experimental variables and discrete representations of chemical structure to the observed target properties. To adequately learn these latent correlations, one would require a model too expensive in complexity to fit on a small dataset. Hierarchical machine learning was developed to embed domain knowledge into the material design problem by transforming features into physico-chemical descriptors that more closely capture the response.[19] The mapping of the original variables to this middle layer of features offers a continuous basis for optimization algorithms and direct physical interpretations of model inputs.

Recently, a HML methodology laid the exploratory groundwork for the prediction of thermal and mechanical properties of polyurethanes by training a model for stress-at-break, strain-at-break, and tan δ of 18 synthesized materials comprised of both linear and crosslinked PU.[20] Pugar et al. extended the goals of HML modeling on TPU beyond simple prediction.[21] Using a standardized method of feature selection via permutation importance, a random forest

model identified correlations among the influential physico-chemical variables that map variations in monomer structure to the glass transition temperature of a TPU. This model demonstrated the utility of statistical learning for identifying key mechanisms that dictate observed trends in properties of complex material systems.

Part of the proposed biSS-TPU model presented here scrutinizes the stability of feature selection for models trained from small libraries of complex materials. Given that small datasets are more likely to have train-test splits which are non-representative of the true data distribution, cases exist where the feature set which achieves the best performance metrics on any given test set may not capture the true physically relevant features. Meinhausen and Buhlmann coined the term *stability selection*, where stability in this case refers to the consistent selection of features regardless of minor changes to a design matrix.[22] In their approach, a sparsifying operator is applied to a candidate feature set with random resampling of subsets from the training data. The frequency of selection for a given feature estimates its posterior selection probability, and it is assumed that the most probable feature set is hypothesized to include the true feature set. In this work, a combined recursive feature elimination-permutation importance repeated over multiple random partitions of the biSS-TPU data is proposed to select a stable subset from a set of middle-layer candidates. This allowed for interpretation of the underlying mechanism governing mixing effects.

Experimental Methods

Thermoplastic Polyurethane Synthesis

A dataset comprised of 76 biSS-TPU and 16 sSS-TPU was synthesized. biSS-TPU diversity depended on a systematic grid search of variations in weight percentage of the hard segment {25%, 35%, 45%, 55%} and biSS phase composition by volume {0.25, 0.5, 0.75} for each binary combination of polyols. An addition 4 biSS-TPU at 45% w%HS were included to confirm the shape of mixing trends.

A set of 4 industrially common polyols were chosen to include miscible pairs from two families, those containing carbonyl-containing repeat units and polyether polyols. The two polyether polyols, polypropylene glycol (PPG) and polytetramethylene ether glycol (PTMEG), were miscible when mixed at 100□C. Carbonyl-containing polyols included a polyester polyol, poly(butylene adipate) glycol (PBA), and a polycarbonate polyol, poly(hexamethylene carbonate) glycol (PHC). Both carbonyl-containing polyols were miscible when mixed at 100□C. However, all pairwise mixtures of carbonyl-containing polyols and polyethers were immiscible at 100□C. All polyols had a 2000 g/mol number-averaged molecular weight. Hard segment composition in all TPU was held constant using 4,4-diphenylmethane diisocyanate (MDI) and butanediol (BDO) chain extender. All TPU were formulated to a 1.05 NCO:OH index. Covestro LLC gifted the supply of MDI, PPG and PHC. Stepan Company gifted the PBA. PTMEG and BDO were purchased from Millipore Sigma.

sSS-TPU and biSS-TPU were synthesized according to a two-step polyaddition copolymerization involving three major components: polyols, MDI, and BDO. In the first step, polyols were reacted with an excess of MDI in an oil bath at 110□C with adequate stirring to form prepolymer isocyanate-terminated urethanes oligomers. For the synthesis of biSS-TPU two polyols were stirred at 110□C according to the appropriate volume fractions based on assigned biSS phase composition. After at least 20 minutes of mixing, MDI was added to the polyol blend. biSS-TPU polyol ratios varied from 1:3, 1:1, and 3:1. In the second step, the pre-polymerization reaction vessel was removed from heat, and a stoichiometrically appropriate amount of BDO was immediately stirred into the prepolymer. The contents of the mixture were

then transferred to a 100x20x2 mm Teflon mold and heated at 100□C for approximately 20 h. to ensure complete cure of the TPU copolymers.

Characterization

Cured TPU were characterized by Fourier-transform infrared spectroscopy (FTIR) using a Frontier Spectrometer (PerkinElmer) in the 4000-700 cm^{-1} range. Characteristics peaks for free isocyanate (2200 cm^{-1}) and polyurea (1690-1640 cm^{-1}) were absent, indicating the synthesis of phase-pure TPU. Wavenumbers at ~1700 cm^{-1} and ~1730 cm^{-1} were recorded to estimate the relative abundance of hydrogen bonded and free carbonyl groups, respectively.

Glass transitions of select TPU were characterized by dynamic scanning calorimetry (DSC) with the TA instruments model DSC 250. During DSC measurements, ~10 mg samples were subjected to a linear heat ramp at 10 □C/min from -70 to 200□C. Hard phase melting points were measured for all tested TPU at approximately 180□C, which is standard for MDI-based TPU. Storage modulus, loss modulus and tan δ profiles were characterized for select TPU formulations by dynamic mechanical analysis (DMA) using the TA Instruments model DMA 850 with an ACS-3 chiller. Samples of approximately 20.0 x 13.8 x (2.00-3.60) mm dimensions were cut from TPU materials. The samples were heated from -80 to 160□C at a linear rate of 3 □C/min. All DSC and DMA data were analyzed using the TRIOS software package.

Values of Young's modulus of samples cut from the synthesized polyurethanes were measured by tensile elongation via a rheometer (TA Instruments model Discovery HR-2) with the film grips accessory at room temperature. Cross-sectional areas of the cut-outs were measured with by hand with a caliper. The strain rate during tensile measurements was kept constant at 0.05 mm/s for all samples. Modulus values were measured by calculating the onset slope of resulting stress-strain curves using the TRIOS software package and averaging over 5 replicates per formulation.

Machine Learning Computations

Machine learning algorithms were implemented using the scikit-learn Python package. The dataset was partitioned according to an 80%/20% train-test split. A workflow was coded to store several model types and respective sets of tunable hyperparameters into dictionaries, such

that multiple model types could be trained with optimized hyperparameters over multiple randomized train-test splits. Model types investigated included the least absolute shrinkage and selection operator (LASSO), kernel ridge regression (KRR), relevance vector machines (RVR), adaboost regression trees (adaboost), gradient-boosted regression trees (Gradboost), and random forests (RF).

Feature selection for each model type involved a multistep procedure involving data visualization, Pearson correlation analysis, and recursive feature elimination (RFE) based on permutation importance (PI) scores over multiple train-test splits. The PI algorithm in scikit-learn refits a model repeatedly with optimized hyperparameters and different permutations of a feature over the dataset, breaking its correlation with the response, and assigning high importance scores for those features which result in diminished model performance when that correlation is absent.[23, 24] Errors in PI can result from the inclusion of redundant features. Therefore, Pearson correlation analysis was necessary to remove collinear features prior to RFE-PI. RFE starts with the full set of candidate features and iteratively removes features until a user-specified number remains. In this work, RFE removed features until only those with the highest PI scores survived.

The candidate feature set consisted of those from several sources: quantum chemical descriptors calculated using density functional theory (DFT), cheminformatics descriptors calculated with the RDKit package in Python, group contribution estimates of Hildebrand solubility parameters, empirical estimates from FTIR spectra, and miscellaneous soft segment descriptors. biSS-TPU descriptors were computed as weighted averages of sSS-TPU or individual polyol properties where weights were appropriate SS phase compositions given as volume fractions of respective polyols out of the total polyol content (e.g. $\phi = 0.25$ would indicate a 1:3 polyol ratio). For the full list of screened features, see the addendum section II.

All DFT calculations were carried out with a B3LYP functional and 6-31G++-G(d,p) basis set using the Gaussian 16W software package at 198.15K. DFT-based polyol descriptors, including chemical hardness estimated from the HOMO-LUMO energy gap and dipole moment, were computed for methyl-terminated polyol repeat units in vacuum. The Pugar feature MPC_HS-MPC_SS was computed for the HS unit (MDI + BDO) units with the polarizable continuum model, such that calculations treated the HS unit as immersed in a solvent of polyol.

Common descriptors for cheminformatics, such as polarizability and octanol-water partition coefficient (logP), were computed in RDKit for simplified molecular-input line-entry system (SMILES) representations of polyol repeat units.

Hildebrand solubility parameters for the repeat units of each polyol were estimated by the Van Krevelen group contribution method using Hoy and Fedors estimates of cohesive energy density.[25] The Hildebrand solubility parameter for MDI was computed by the Stefanis et al.[26, 27] group contribution estimates in a method consistent with that of Wenning et al.[16]

$$\delta_{Hoy} = \frac{\sum_i F_i}{\sum_i V_{m,i}}$$

$$\delta_{Fedors} = \left(\frac{\sum_i E_{coh,i}}{\sum_i V_{m,i}}\right)^{\frac{1}{2}}$$

$$\delta_{Stefanis} = \left(\sum_i n_i F_i + \sum_j m_j S_j + 75954.1\right)^{0.383837} - 56.14$$

Miscellaneous common polymer attributes, such as degree of polymerization, were acquired from manufacturer technical reports. Polyol T_g and T_m were measured by DSC. The prepolymer degree of polymerization (PP_DP) following Flory statistics of step-growth polymerizations was calculated with the following formula[13]:

$$DP_{PP} = \lim_{p\to 1} \frac{1+r}{1+p-2rp} = \frac{1+r}{1-r} = \frac{1+\frac{eq_{OH}}{eq_{NCO}}}{1-\frac{eq_{OH}}{eq_{NCO}}}$$

Where r is the equivalence ratio of hydroxyl (OH) functional groups to isocyanate functional groups (NCO) in an excess of diisocyanate, and p is conversion. Because the PP_DP was incapable of distinguishing among biSS-TPU formulations, a descriptor which counts the number of covalent bonds in a prepolymer backbone was calculated. This included covalent bonds of polyol backbones. The four polyols each had unique degrees of polymerization because chain size was standardized by number-averaged molecular weight.

$$Avg\ Tot\_NumBonds\_PP = (DP_{PP} - 1) + \frac{DP_{PP} - 1}{2}[\phi_A(DP_A - 1) + \phi_B(DP_B - 1)]$$

The lefthand term counts urethane linkages formed from NCO and OH functional groups. The righthand term calculates the average number of bonds in the backbone of polyols A and B, weighted by the SS phase composition given as volume fraction out of the total SS content. The righthand multiplicative pre-factor counts the total number of polyols in the prepolymer chain.

Results

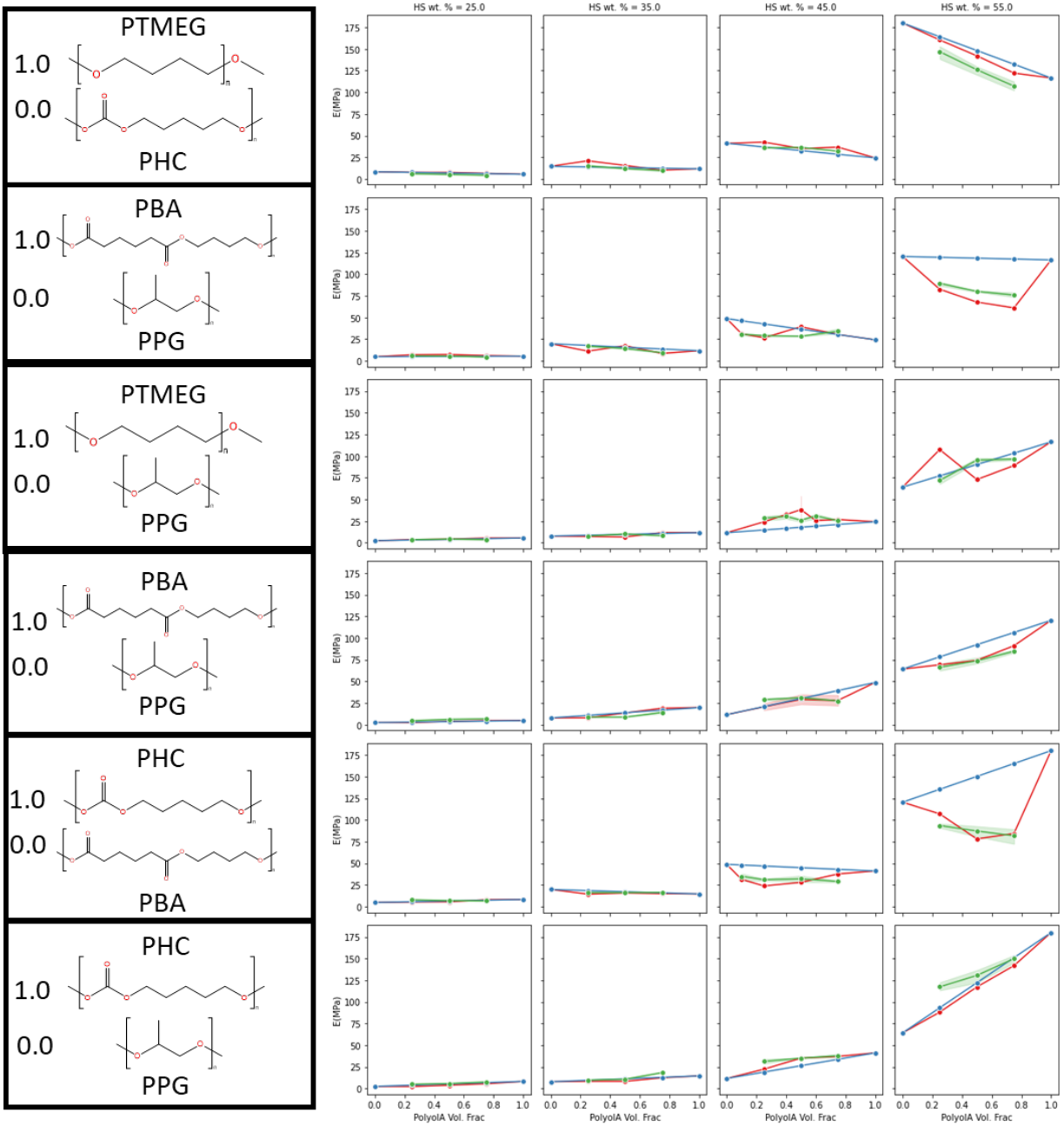

Figure 3 Young's modulus verses soft phase composition given as volume fraction of a polyol in the soft phase. (Red) Measured modulus values of biSS-TPU & sSS-TPU controls. (Blue) average biSS-TPU modulus weighed by soft phase composition to show expected values in the absence of mixing effects (Green) predictions of biSS-TPU modulus of a RF with RFE-PI features accumulated over 30 random train-test splits.

Mixing effects in biSS-TPU were defined as the residual of the measured Young's modulus after subtracting the weighted average modulus of corresponding sSS-TPU controls. The weights were soft phase compositions, ϕ (i.e. ϕ = 0.5 is equivalent to a 1:1 volume ratio of polyol A and B).

$$Mixing\ Effect = E_{Residual} = E - (\phi_A E_A + \phi_B E_B)$$

Figure 3 shows that mixing effects were observed in the synthesized library of biSS-TPU elastomers, and that mixing effects increase with the weight percentage of hard segment content (w%HS). In fact, strong mixing effects were only observed at the highest w%HS, 55%. Nearly all instances of mixing effects decreased the modulus compared to the corresponding controls, with the exception of PTMEG and PPG biSS combinations with a PPG majority.

Of the 76 biSS-TPU materials, mixing effects were observed in only 18 instances with high w%HS and specific polyol combinations. Therefore, HML models were trained to predict the moduli rather than mixing effect. A HML model was trained from both biSS-TPU and sSS-TPU controls, with the assertion that the model can successfully predict biSS-TPU modulus only if it effectively learns mixing effects. The following demonstrates a proposed workflow used to train a random forest to learn mixing effects in order to predict the modulus of a biSS-TPU.

In this work, selection of a model type and sparse feature set occurred over multiple steps, each involving an evaluation over multiple randomized train-test splits to evaluate stability when trained on a small dataset. Model types included the least absolute shrinkage and selection operator (LASSO), kernel ridge regression (KRR), relevance vector machines (RVR), adaboosted regression trees (AdaBoost), gradient boosted trees (GradBoost), and random forests (RF). This set provided a diaspora of model families ranging from regularized linear regression to kernelized methods to ensembles of decision trees. Out of the 6 investigated model types, random forests performed the best with respect to predictive strength and evidence of learning mixing effects in bi-SS TPU. Addendum Section I provides a description of each model type.

The primary challenge in modeling with small scientific data was to choose a subset of physically interpretable features that are most relevant for predicting a target property. All candidate features were calculated as averages of polyol or sSS-TPU properties weighted by ϕ. Thirty-four features were generated from polyol descriptors computed with RDKit, DFT, group

contribution estimates of solubility parameters, or empirical characterization techniques. Seven features were obtained from a collaboration with Joseph Pugar of the Washburn laboratory based on a working model to predict the moduli of sSS-TPU from a material library with a broader chemical diversity. A list of all candidate features and sources is provided in the Addendum section II.

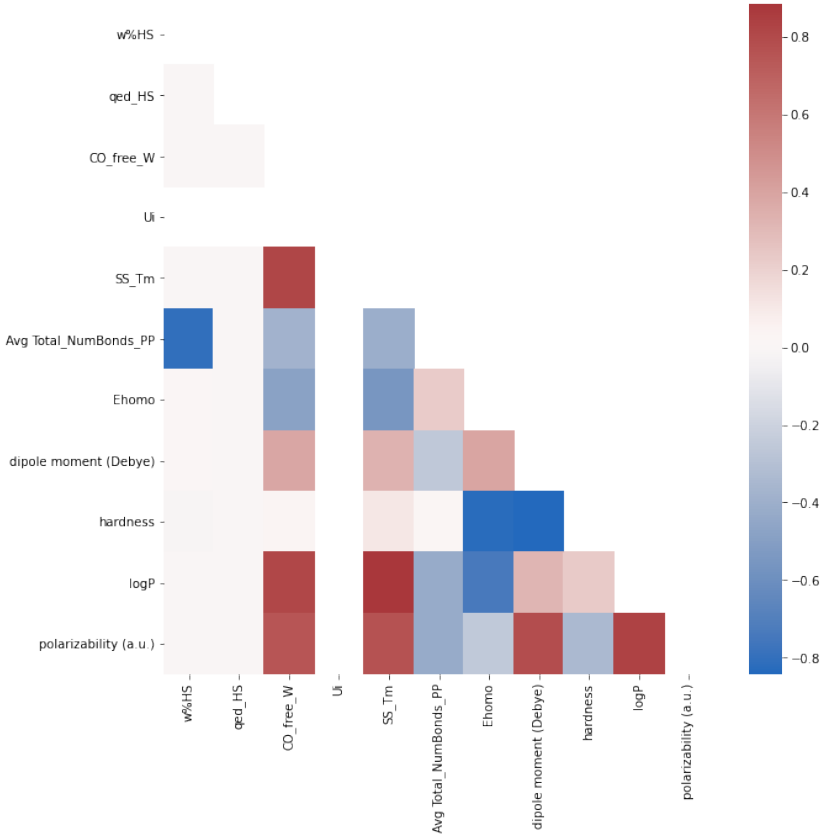

Figure 4. Correlation matrix after screening out features with pairwise Pearson correlation coefficients > 0.9

Sparse sets of 3-5 features were selected for each model type using a combined recursive feature elimination and permutation importance (RFE-PI) algorithm. A screening of Pearson correlation coefficients removed all but the 11 features in figure 4. For pairs of features which shared a high absolute Pearson correlation coefficient (>0.90), the feature with the lowest correlation with the modulus was removed. Afterwards, RFE-PI was repeated over a range of 3-6 selected features for 15 randomized train-test splits. Figure 5 displays the frequency of selection per feature with the assumption that the most physically relevant features would be selected most frequently by RFE-PI on randomized partitions of the dataset. The following feature set was

selected for random forest: **w%HS**, **Avg Total_NumBonds_PP**, and polyol monomer **dipole moment.**

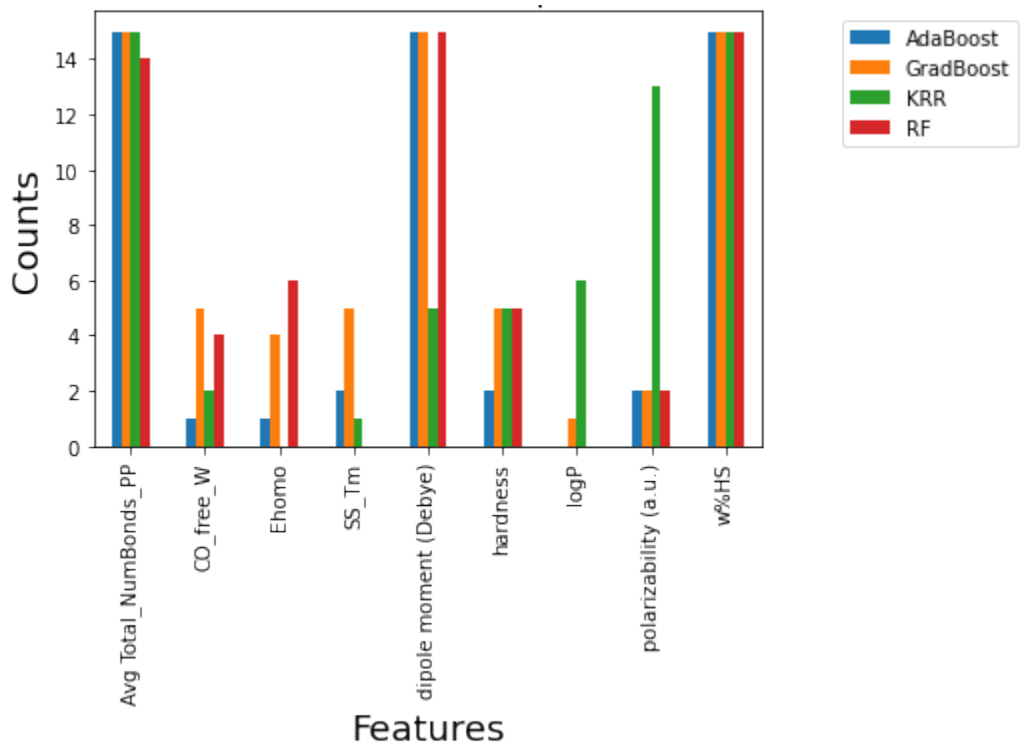

Figure 5. The most frequently selected features from the best performing models per model type and per train-test split accumulated over 15 random train-test splits. LASSO and RVR models were excluded due to poor predictive performance.

Figure 6 shows the distribution of mean squared error (MSE) and coefficient of determination (R^2) scores of a RF trained with the RFE-PI feature set over 30 random train-test splits. Figure 7 presents the predicted-actual plots of the median MSE_{test} split. Due to the small dataset size and disparate mixing effects, test scores tended to have wider distributions than training scores. Although AdaBoost, KRR, and RF models had similar average and median test scores, RF was the most stable model type with the narrowest test score distributions.

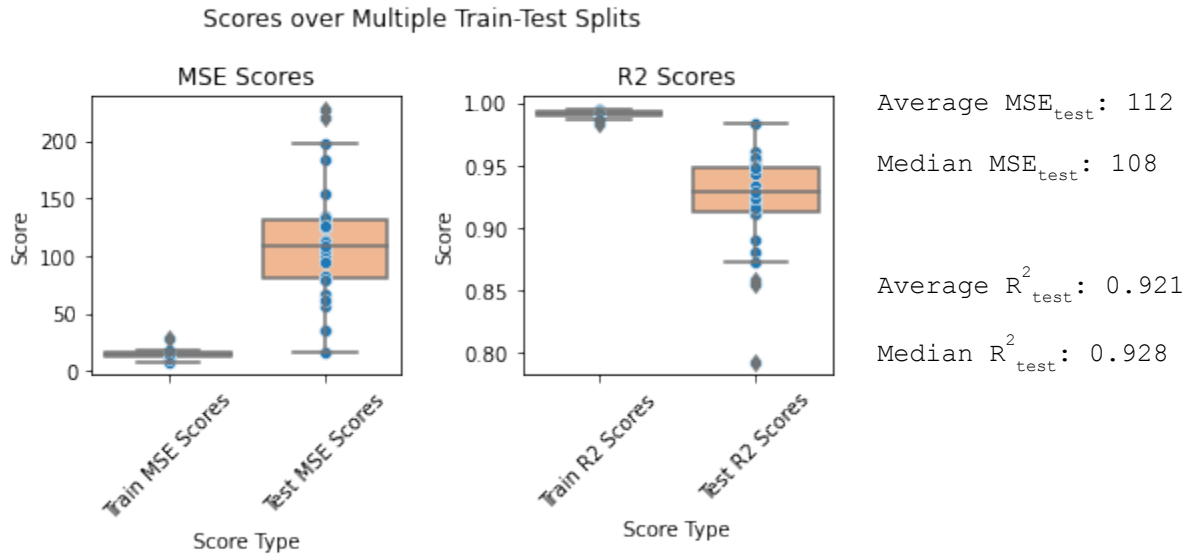

Figure 6 Distribution of MSE and R^2 scores for RF train with sparse RFE-PI features

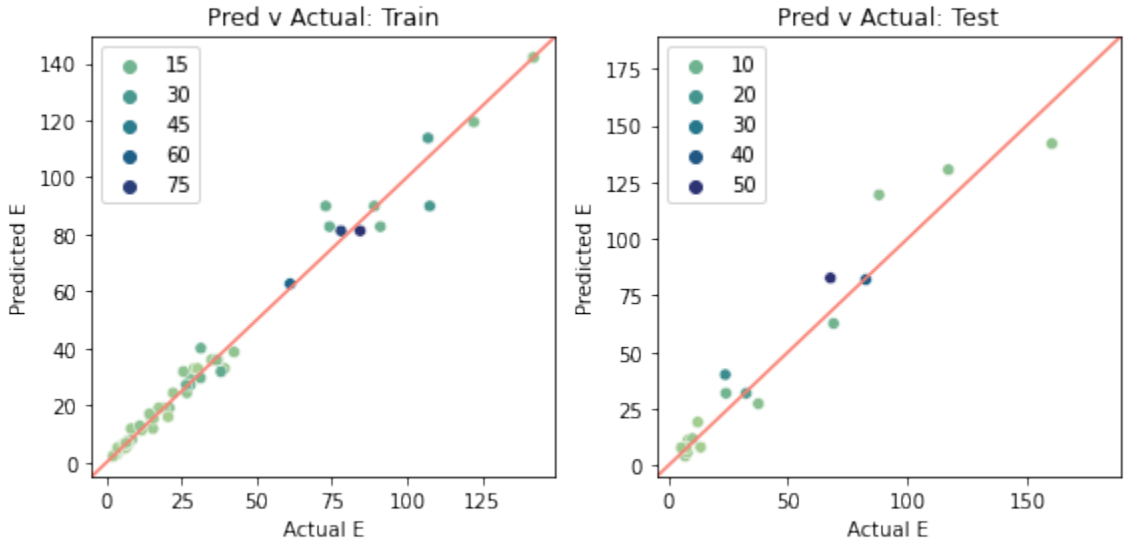

Figure 7. Predicted-Actual plot for the train-test split with median MSE for RF model. Color is mapped to mixing effect and E is Young's modulus in MPa.

Modulus values of biSS-TPU predicted by the RF model with RFE-PI features over 30 train-test splits are plotted in figure 3 as green points. The optimized model demonstrated the ability to learn general mixing effects, except for the combination of PTMEG and PPG polyols where the unusual instance of enhanced modulus was observed at a ratio of 3:1 PPG:PTMEG. One explanation for this outlier, could be soft phase crystallinity. It is known that soft segment crystallization, which has been observed for these and similar polyether soft phases, can enhance the modulus of a PU by acting as an effective secondary hard phase.[12, 28] For instance, PEO-

PPO-PEO copolymer soft segment units resulted in enhanced toughness of a polyurethane, which was attributed to increased soft segment crystallization.[29]

In a final step, the optimized feature set was assessed by relative importance to the learning of mixing effects. The strongest mixing effects were observed for biSS-TPU at 55% weight percent of hard segment content (w%HS). Therefore, permutation importance scores were averaged for models trained on only 55% w%HS data over 10 random train-test splits. In general, a machine learning algorithm needed to learn two trends to predict biSS-TPU modulus: hard segment effect and mixing effects for distinct polyol combinations. By training on only 55% w%HS, PI can provide relative importance scores for the latter. For both AdaBoost and RF ensembled tree-based methods, polyol dipole moment PI scores were significantly higher than the expected number of bonds in a prepolymer backbone (Avg Total_NumBonds_PP). RFE-PI selected an additional two features for KRR, the octanol-water partition coefficient (logP) and chemical hardness. Dipole moment and Avg Total_NumBonds are not significantly different for KRR, but the pair is significantly different from the pair of logP and hardness. Error bars represent 95% confidence intervals estimated by the bootstrap method.

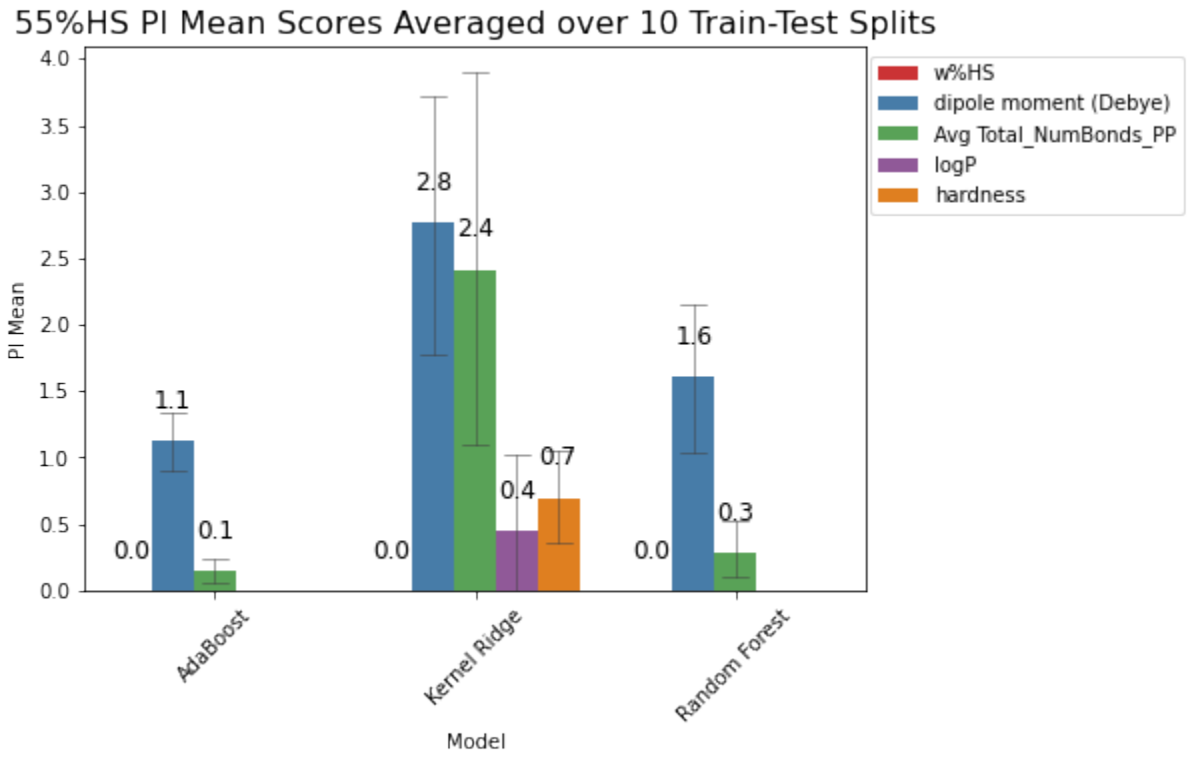

Figure 8. Permutation Importance Scores for AdaBoost, KRR, and RF models that were trained on only 55% w%HS data

Ultimately, when interpreting the RFE-PI features, one must consider how mixing of soft phase polyols may influence the behavior at the hard-soft phase interface. Recall that TPU can be considered LMBCP. Garret et al. observed that at high w%HS (40-70%) TPU may cure so rapidly that the prepolymer mixture may become locked in place as vitrification slows the rate of phase separation.[30] Under the assumption of reaction-induced phase separation, the degree of segregation in a blocked prepolymer would be dictated by both the polar incompatibility of the polyols and the solvating effect of free diisocyanate molecules. A higher w%HS formulation would have a higher prepolymer NCO:OH index, such that the free diisocyanate molecules would promote miscibility of the SS block units. Once rapidly cured in place, a dispersed hard segment mesophase would form with SS blocks trapped in proximity, depending on the extent of separation of prepolymer blocks and, in turn, on the polar interaction of the two polyols. Statistically, the greatest extent of regional irregularity would take place at $\phi = 0.5$ where the greatest mixing effects tended to be observed.

The phase behavior of LMBCP melts was found to behave similarly to those of diblock copolymers.[14] In the case that vitrification kinetics compete with phase separation at high w%HS, a weakened phase segregation implies a stronger dependence on χ*DP. A dipole moment reflects asymmetry in the distribution of electron density across a molecule. Thus, the polyol dipole moment would reflect polar enthalpic interactions between polyols. For the selected four polyols (two polyethers, a polyester, and a polycarbonate polyol), the dipole moment was governed by the density of ether and carbonyl function groups. Avg_NumRotBonds_PP provided an estimate of the effective SS unit degree of polymerization that can distinguish between binary soft segment combinations. This is an artefact of the polyols being standardized by molecular weight, rather than degree of polymerization, such that carbonyl containing polyols tend to have significantly lower degrees of polymerization. Thus, each of the four polyols and each combination of polyols had a unique average degree of polymerization.

Next Steps

To gauge the efficacy of the biSS-TPU predictive model, a validation set of biSS-TPU with hydrogenated MDI will be synthesized with the binary polyol combinations which resulted in mixing effects. In collaboration with Joseph Pugar of the Washburn group, the model will combine sSS-TPU and biSS-TPU descriptors to train a model using the RFE-PI feature selection workflow proposed in this work. The task at hand will be to predict the modulus of unknown biSS-TPU when trained on a joint dataset which merges the biSS-TPU of this work with a more chemically diverse sSS-TPU library synthesized by Pugar. When combined with a sSS-TPU library, the 18 instances of strong mixing effects would effectively be diluted. A few strategies for balancing datasets in machine learning have been proposed. An undersampling algorithm would randomly remove instances from uninteresting regions of the fitted chemical space to improve emphasis on the biSS-TPU that exhibit mixing effects. Alternatively, an oversampling method would synthesize hypothetical instances of mixing effects based on nearest-neighbor interpolation. SMOGN (synthetic minority oversampling with Gaussian noise) would regulate both strategies to balance the combined TPU dataset, and an opensource Python implementation is readily available.[31]

Conclusions

A library of 76 bi-SS TPU were synthesized along with 16 sSS-TPU controls. Upon comparison of measured modulus values, biSS-TPU mixing effects were observed at high hard segment content (>35 wt.%) for certain polyol combinations. In the absence of mixing effects, the modulus was observed to follow the average modulus of sSS-TPU controls, weighted by volume fraction composition of the polyol components in the soft phase. Typically, mixing effects decreased modulus, and this was hypothesized to be due to a dispersion of the pure hard phase into a mesophase consisting of segments of the two soft phase units and hard phase units. One combination of two polyether polyols, PTMEG and PPG, resulted in rare cases of enhanced modulus values. This was hypothesized to result from reinforcement due to soft phase crystallization.

This work proposed a machine learning workflow to learn mixing effects in biSS-TPU in order to accurately predict Young's modulus. Several machine learning model types were investigated in a workflow designed to standardize feature selection on a small material dataset. The RFE-PI algorithm was implemented as a model-agnostic approach to assigning relative feature importance, and it was repeated over multiple random 0.8/0.2 train-test splits such that feature selection could be compared across multiple model types and be robust to small changes in the training set. Based on this workflow, a random forest trained with three features (**w%HS**, **Avg Total_NumBonds_PP**, and polyol repeat unit **dipole moment)** achieved high predictive scores. The dipole moment feature proved to contribute the most to the learning of mixing effects at high hard segment content. The final stage necessary for completion of this project would synthesize a validation set consisting of biSS-TPU with new chemical compositions that would assess the generalizability of the physical trends learned in the random forest model.

Work Cited

(1) Das, A.; Mahanwar, P. A Brief Discussion on Advances in Polyurethane Applications. *Adv. Ind. Eng. Polym. Res.* **2020**, *3* (3), 93–101. https://doi.org/10.1016/j.aiepr.2020.07.002.

(2) Cooper, S. L.; Tobolsky, A. V. Properties of Linear Elastomeric Polyurethanes. *J. Appl. Polym. Sci.* **1966**, *10* (12), 1837–1844. https://doi.org/10.1002/app.1966.070101204.

(3) Misha, A.; Maiti, P. Morphology of Polyurethanes at Various Length Scales: The Influence of Chain Structure. *J. Appl. Polym. Sci.* **2011**, *120* (6), 3546–3555.

(4) Cho, J. W.; Jung, Y. C.; Chung, Y.-C.; Chun, B. C. Improved Mechancial Properties of Shape-Memory Polyurethane Block Copolymers through the Control of the Soft-Segment Arrangement. *J. Appl. Polym. Sci.* **2004**, *93* (5), 2410–2415.

(5) Chung, Y. C.; Regen, S. L. Communications to the Editor. *Macromolecules* **1991**, *24* (20), 5738–5739. https://doi.org/10.1021/ma00020a042.

(6) Queiroz, D. P.; Botelho do Rego, A. M.; de Pinho, M. N. Bi-Soft Segment Polyurethane Membranes: Surface Studies by X-Ray Photoelectron Spectroscopy. *J. Memb. Sci.* **2006**, *281* (1–2), 239–244. https://doi.org/10.1016/j.memsci.2006.03.037.

(7) Zhao, C. T.; Norberta De Pinho, M. Design of Polypropylene Oxide/Polybutadiene Bi-Soft Segment Urethane/Urea Polymer for Pervaporation Membranes. *Polymer (Guildf).* **1999**, *40* (22), 6089–6097. https://doi.org/10.1016/S0032-3861(98)00833-7.

(8) Liu, Y.; Liu, L.; Liang, Y. Relationship between Structure and Dynamic Mechanical Properties of Thermoplastic Polyurethane Elastomer Containing Bi-Soft Segment. *J. Appl. Polym. Sci.* **2020**, *137* (45), 1–9. https://doi.org/10.1002/app.49414.

(9) Wen, T.-C.; Fang, J.-C.; Gopalan, A. Morphology and Conductivity Changes in a Thermoplastic Polyurethane-Based Copolymer Consisting of Different Soft Segments. *J. Appl. Polym. Sci.* **1985**, *82* (6), 1462–1473.

(10) Gunatillake, P. A.; Meijs, G. F.; McCarthy, S. J.; Adhikari, R. Poly(Dimethylsiloxane)/Poly(Hexamethylene Oxide) Mixed Macrodiol Based

Polyurethane Elastomers I. Synthesis and Properties. *J. Appl. Polym. Sci.* **2000**, *76* (14), 2026–2040.

(11) Ginzburg, V. V.; Bierano, J.; Christenson, C. P.; Schrock, A. K.; Patashinksi, A. Z. No Title. *J. Polym. Sci. B Polym. Phys.* **2007**, *45* (16), 2123–2135.

(12) Bates, F. S.; Fredrickson, G. H. Block Copolymers-Designer Soft Materials. *Phys. Today* **1999**, *52* (2), 32–38. https://doi.org/10.1063/1.882522.

(13) Hiemenz, P. C.; Lodge, T. *Polymer Chemistry 2nd Ed*; 2007.

(14) Fuensanta, M.; Martín-Martínez, J. M. Structural and Viscoelastic Properties of Thermoplastic Polyurethanes Containing Mixed Soft Segments with Potential Application as Pressure Sensitive Adhesives. *Polymers (Basel).* **2021**, *13* (18). https://doi.org/10.3390/polym13183097.

(15) Wenning, C.; Schmidt, A. M.; Leimenstoll, M. C. Evolution of Reaction-Induced Phase Segregations in Bi-Soft Segment Urethane Oligomers. *Macromol. Chem. Phys.* **2020**, *221* (5), 1900458.

(16) Wenning, C.; Barbe, S.; Achten, D.; Schmidt, A. M.; Leimenstoll, M. C. Prediction of Initial Miscibility for Ternary Polyurethane Reaction Mixtures on Basis of Solubility Parameters and Flory–Huggins Theory. *Macromol. Chem. Phys.* **2018**, *219* (5), 1–8. https://doi.org/10.1002/macp.201700544.

(17) Chen, L.; Pilania, G.; Batra, R.; Huan, T. D.; Kim, C.; Kuenneth, C.; Ramprasad, R. Polymer Informatics: Current Status and Critical next Steps. *Mater. Sci. Eng. R Reports* **2021**, *144* (December 2020), 100595. https://doi.org/10.1016/j.mser.2020.100595.

(18) Pollice, R.; Dos Passos Gomes, G.; Aldeghi, M.; Hickman, R. J.; Krenn, M.; Lavigne, C.; Lindner-D'Addario, M.; Nigam, A.; Ser, C. T.; Yao, Z.; Aspuru-Guzik, A. Data-Driven Strategies for Accelerated Materials Design. *Acc. Chem. Res.* **2021**, *54* (4), 849–860. https://doi.org/10.1021/acs.accounts.0c00785.

(19) Menon, A.; Gupta, C.; Perkins, K. M.; Decost, B. L.; Budwal, N.; Rios, R. T.; Zhang, K.; Póczos, B.; Washburn, N. R. Elucidating Multi-Physics Interactions in Suspensions for the Design of Polymeric Dispersants: A Hierarchical Machine Learning Approach. *Mol. Syst.*

Des. Eng. **2017**, *2* (3), 263–273. https://doi.org/10.1039/c7me00027h.

(20) Menon, A.; Thompson-Colón, J. A.; Washburn, N. R. Hierarchical Machine Learning Model for Mechanical Property Predictions of Polyurethane Elastomers from Small Datasets. *Front. Mater.* **2019**, *6* (May), 1–12. https://doi.org/10.3389/fmats.2019.00087.

(21) Pugar, J. A.; Childs, C. M.; Huang, C.; Haider, K. W.; Washburn, N. R. Elucidating the Physicochemical Basis of the Glass Transition Temperature in Linear Polyurethane Elastomers with Machine Learning. *J. Phys. Chem. B* **2020**, *124* (43), 9722–9733. https://doi.org/10.1021/acs.jpcb.0c06439.

(22) Meinshausen, N.; Bühlmann, P. Stability Selection. *J. R. Stat. Soc. Ser. B Stat. Methodol.* **2010**, *72* (4), 417–473. https://doi.org/10.1111/j.1467-9868.2010.00740.x.

(23) Jin, Z.; Shang, J.; Zhu, Q.; Ling, C.; Xie, W.; Qiang, B. RFRSF: Employee Turnover Prediction Based on Random Forests and Survival Analysis. *Lect. Notes Comput. Sci. (including Subser. Lect. Notes Artif. Intell. Lect. Notes Bioinformatics)* **2020**, *12343 LNCS*, 503–515. https://doi.org/10.1007/978-3-030-62008-0_35.

(24) Tong, J.; Zhang, J.; Dong, E.; Du, S. Severity Classification of Parkinson's Disease Based on Permutation-Variable Importance and Persistent Entropy. *Appl. Sci.* **2021**, *11* (4), 1–20. https://doi.org/10.3390/app11041834.

(25) Van krevelen, D. W.; Nijenhuis, K. TE. *Properties of Polymers: Their Correlation with Chemical Structure; Their Numerical Estimation and Prediction From Additive Group Contributions 4th Ed.*; 2009.

(26) Stefanies, E.; Constantinou, L.; Panayiotou, C. A Group-Contribution Method for Predicting Pure Component Properties of Biochemical and Safety Interest. *Ind. Eng. Chem. Res.* **2004**, *43* (19), 6253–6261. https://doi.org/10.1021/ie0497184.

(27) Stefanis, E.; Panayiotou, C. Prediction of Hansen Solubility Parameters with a New Group-Contribution Method. *Int. J. Thermophys.* **2008**, *29* (2), 568–585. https://doi.org/10.1007/s10765-008-0415-z.

(28) Sonnenschein, M. F.; Lysenko, Z.; Brune, D. A.; Wendt, B. L.; Schrock, A. K. Enhancing Polyurethane Properties via Soft Segment Crystallization. *Polymer (Guildf).* **2005**, *46*

(23), 10158–10166. https://doi.org/10.1016/j.polymer.2005.08.006.

(29) Korley, L. S. T. J.; Pate, B. D.; Thomas, E. L.; Hammond, P. T. Effect of the Degree of Soft and Hard Segment Ordering on the Morphology and Mechanical Behavior of Semicrystalline Segmented Polyurethanes. *Polymer (Guildf).* **2006**, *47* (9), 3073–3082. https://doi.org/10.1016/j.polymer.2006.02.093.

(30) Garrett, J. T.; Runt, J.; Lin, J. S. Microphase Separation of Segmented Poly(Urethane Urea) Block Copolymers. *Macromolecules* **2000**, *33* (17), 6353–6359. https://doi.org/10.1021/ma000600i.

(31) Branco, P.; Ribeiro, R. P.; Torgo, L.; Krawczyk, B.; Moniz, N. SMOGN: A Pre-Processing Approach for Imbalanced Regression. *Proc. Mach. Learn. Res.* **2017**, *74*, 36–50.

(32) Zhang, Y.; Ling, C. A Strategy to Apply Machine Learning to Small Datasets in Materials Science. *npj Comput. Mater.* **2018**, *4* (1), 28–33. https://doi.org/10.1038/s41524-018-0081-z.

(33) Aguirresarobe, R. H.; Nevejans, S.; Reck, B.; Irusta, L.; Sardon, H.; Asua, J. M.; Ballard, N. Progress in Polymer Science Healable and Self-Healing Polyurethanes Using Dynamic Chemistry. *Prog. Polym. Sci.* **2021**, *114*, 101362. https://doi.org/10.1016/j.progpolymsci.2021.101362.

(34) Gadwal, I. A Brief Overview on Preparation of Self-Healing Polymers and Coatings via Hydrogen Bonding Interactions. *Macromol* **2020**, *1* (1), 18–36. https://doi.org/10.3390/macromol1010003.

(35) Amamoto, Y.; Otsuka, H.; Takahara, A.; Matyjaszewski, K. Self-Healing of Covalently Cross-Linked Polymers by Reshuffling Thiuram Disulfide Moieties in Air under Visible Light. *Adv. Mater.* **2012**, *24* (29), 3975–3980. https://doi.org/10.1002/adma.201201928.

(36) Zhang, L.; Chen, L.; Rowan, S. J. Trapping Dynamic Disulfide Bonds in the Hard Segments of Thermoplastic Polyurethane Elastomers. *201600320*, 1–10. https://doi.org/10.1002/macp.201600320.

(37) Pilania, G.; Iverson, C. N.; Lookman, T.; Marrone, B. L. Machine-Learning-Based

Predictive Modeling of Glass Transition Temperatures: A Case of Polyhydroxyalkanoate Homopolymers and Copolymers. *J. Chem. Inf. Model.* **2019**, *59* (12), 5013–5025. https://doi.org/10.1021/acs.jcim.9b00807.

(38) Ouyang, R.; Curtarolo, S.; Ahmetcik, E.; Scheffler, M.; Ghiringhelli, L. M. SISSO: A Compressed-Sensing Method for Identifying the Best Low-Dimensional Descriptor in an Immensity of Offered Candidates. *Phys. Rev. Mater.* **2018**, *2* (8), 1–12. https://doi.org/10.1103/PhysRevMaterials.2.083802.

(39) Greenhill, S.; Rana, S.; Gupta, S.; Vellanki, P.; Venkatesh, S. Bayesian Optimization for Adaptive Experimental Design: A Review. *IEEE Access* **2020**, *8*, 13937–13948. https://doi.org/10.1109/ACCESS.2020.2966228.

Addendum

I. Brief Descriptions of Model Types

Adapted from "Machine Learning: A Probabilistic Perspective" by Kevin P. Murphy[1]

Introduction to Machine Learning Practices

Experimentalists collect N instances of data, **D**, in the form of tuples that pair a set of inputted feature vectors, $\mathbf{x_i}$, to a measured output property, y_i.

$$\boldsymbol{D} = (\{\boldsymbol{x_i}, y_i\}, i = 1{:}N)$$

Machine learning algorithms can be trained and adapted to the nuanced trends of that data by fitting a hypothesized function and corresponding parameters, θ, which maps from the set of inputs, **X**, to the outputs, **y**. Therefore, model predictions, $\widehat{\boldsymbol{y}}$, can be computed as follows:

$$\widehat{\boldsymbol{y}} = f(\boldsymbol{x}, \theta)$$

Many models considered in this work rely on an additivity assumption of the functions, such that predictions can be rewritten for a k-feature model as follows:

$$\widehat{\boldsymbol{y}} = f(\boldsymbol{x}, \theta) = \sum_{j=1}^{k} f(\boldsymbol{x}, \theta_j)$$

The problem to be solved in machine learning is to select the most appropriate function from the set of all possible functions. If the function takes on a hypothesized parametric form, then this problem simplifies to finding the set of parameters that best fit the trends observed in the data.

Probabilistically, this problem can be expressed as a posterior distribution, which can be factored into a prior distribution and a likelihood.

$$p(\theta|D) = p(\theta)p(D|\theta)$$

The most common method for choosing the best function is to select the function with the highest posterior probability. For a parametric model, this can be interpreted as finding the set of parameters which is most consistent with the data. To do so, a prior is set over the parameters to

express a priori beliefs about the parameters, and a likelihood is set to reflect the information learned from the data. Given enough data, the poster distribution would have a sharp peak at its maximum. In small data modeling, however, the posterior distribution would have a broad spread, suggesting higher uncertainty in the chosen set of parameters, and in turn the chosen model. For non-parametric models, the problem can be generalized to distributions over function spaces rather than parameter spaces.

Least Squares Linear Regression

The simplest and historically most well-studied model type is linear regression. It assumes the highly restrictive assumption that the observed trends take on a linear structure. In cases where this assumption is valid, one can simply select the proper coefficients in a weighted sum of features to fit the model. This is expressed in matrix notation as follows:

$$\hat{\boldsymbol{y}} = \boldsymbol{X}\boldsymbol{w}$$

The strategy to solve linear regression is to assume a uniform prior (no prior beliefs about the values of the coefficients) and to maximize the likelihood. This turns out to be equivalent to minimizing the loss function known as residual sum of squares (RSS), where residuals are the differences between predictions and observed outputs.

$$RSS(w) = \sum_{i=1}^{N} (y_i - \boldsymbol{x}_i^T \boldsymbol{w})^2$$

RSS provides the convenience of a convex optimization problem. Linear regressions enjoy short computation times, because the best choice of coefficients has a closed form solution:

$$\boldsymbol{w^{LS}} = (\boldsymbol{X^T X})^{-1} \boldsymbol{X^T y}.$$

Lease Absolute shrinkage and Selection Operator

The problem with maximum likelihood estimates, is that they tend to overfit the data. Usually, in machine learning this results in a model with too many features which are either redundant with pre-existing features of the model or merely lacking in any useful information at

all. Strengthening the prior distribution steals weight away from the likelihood, thus controlling the extent to which the fitted model tries to capture the minor nuances of the data. The Least Absolute Shrinkage and Selection Operator (LASSO) is a least squares linear regression with a Laplace prior distribution. This results in the optimization problem of minimizing the RSS while penalizing by the L_1-norm of feature coefficients. The Lagrange form of this optimization is given as follows:

$$J(w) = RSS(w) + \lambda\left|\left|\boldsymbol{w}\right|\right|_1$$

While other forms of the penalty have been proposed, LASSO works well with small datasets because the L_1-norm can drive the coefficients of unimportant features to zero, effectively removing them from the model.

Kernel Ridge Regression

Linear regression and LASSO are only capable of fitting linear functions. The strategy to allow linear models to fit non-linear trends is to transform the feature set into a new set of non-linear features. This is still considered linear regression, because only the linearity of parameters matter. One successful choice of basis expansions is to use a set of kernelized functions as the model inputs. Kernel functions, in this case, can be thought of as extensions of inner products to higher dimensional function spaces. The contribution of kernels is often interpreted as a generalization of the inner product as a metric of similarity. That is, the elementary property of inner products from the law of cosines states that $\boldsymbol{a^T b} = \left|\left|\boldsymbol{a}\right|\right|\left|\left|\boldsymbol{b}\right|\right|\cos(\theta)$. Here, $\cos(\theta)$ gives a value from the interval, [-1,1], which indicates the extent of coalignment between vectors, $\boldsymbol{a}$ and $\boldsymbol{b}$. When using kernels, the assumption follows that if two input coordinates in the feature space are similar, then the outputs must also be similar.

Kernel ridge regression (KRR) is a common example of a vector machine, a linear model with a kernelized feature set, and KRR generally performs well on small datasets. It is essentially a kernelized extension of ridge regression, which is similar to LASSO except it assumes a Gaussian prior and implements an L_2-norm penalty.

$$J(w) = RSS(w) + \lambda\left|\left|\boldsymbol{w}\right|\right|_2$$

After some amount of linear algebra, the solution to kernelized vector machines usually comes out as a sum of kernel functions weighted by dual variables.

$$\hat{\boldsymbol{y}} = \sum_{i=1}^{N} \alpha_i \boldsymbol{x}_i^T \boldsymbol{x} = \sum_{i=1}^{N} \alpha_i \kappa(\boldsymbol{x}, \boldsymbol{x}_i)$$

where

$$\boldsymbol{\alpha} \triangleq (\mathbf{K} + \lambda \boldsymbol{I}_N)^{-1} \boldsymbol{y}$$

Relevance vector machines

KRR uses a non-sparse kernel set, but the performance and computation time of vector machines can sometimes be improved by sparsifying the kernels. The most common type of sparse kernel vector machine is called the support vector machines (SVM), which famously model nonlinear functions on small datasets when taking advantage of the so-called kernel trick. This work opted to use relevance vector machines (RVR) instead because attempts to implement the current rendition of RFE-PI code with support vector machines in scikit-learn crashed. Nonetheless, RVR has been noted to provide similar results to SVM. Because RVR is a probabilistic method, it can offer certain advantages over SVM. Although the computation time of a single RVR model is higher than that of an SVM, a workflow using RVR often computes quicker because SVM's require cross-validation of hyperparameters whereas RVR fits hyperparameters with an empirical Bayesian method. Traditionally, this method was an algorithm known as autonomous relevance detection. In practice, people use a greedy algorithm.

Adaboost and Gradient Boost

Boosting refers to a sequential ensemble method. In an ensemble method, multiple base models are fit on bootstrapped subsets of the training data, and their predictions are combined to make a final prediction. The advantage of ensemble methods follows with Sir Francis Gaolton's notion of the "wisdom of the crowd." In the same way that the median or average estimate of an ox's weight from a crowd of amateurs can outperform the guess of an ox expert, the weighted estimate of many weak models can often outperform the estimate of a singular strong model. In boosting, weak base models are fit iteratively over each data instance with a weight assigned to

each data instance that penalizes instances with incorrect predictions. In each iteration, the weights are adjusted so that data instances that are more difficult to predict have increasing importance in each successive generation. Adaboost refers to a boosting algorithm with a negative exponential loss function. Gradient boosting was proposed as a more general scheme. By rewriting the optimization problem associated with boosting as a gradient descent problem over a space of functions, gradient boosting could be generalized to multiple types of loss functions. Boosting models in scikit-learn use simple regression trees as the base models by default.

Random Forests

A random forest is an ensemble method that aggregates predictions from multiple regression trees, each fit on a bootstrap subset of the data. Regression trees partition a feature space into compartmentalized regions with iterative binary splits. The estimate of the response variable in each region is the localized average response of that region. Regression trees may offer good predictive strength and interpretable results, but they also suffer from an inherent risk of instability. The hierarchical structure of a graphical tree makes it susceptible to large-scale changes in its structure from a small change to the dataset. If the change is such that only the partition associated with a leaf (terminal node) is altered, then there is a minor change to the tree structure. However, if the change requires an alteration in a node closer to the root of the tree, then an entire subtree may require reworking. To overcome this instability, bootstrap aggregated (bagged) trees were introduced, which averages predictions from multiple regression trees, each modeled on a bootstrap sampled subset of the training data. The issue with bagging is that each base tree would have a correlated structure. Random forests improve upon bagged trees by allowing each base tree to be trained on a randomly permuted subset of features. Although random forests often achieve high prediction accuracies, their complex structure requires the most degrees of freedom out of every model considered in this work.

II. Feature Set Description

Candidate Feature Name	***Acronym***	***Source***
Hard segment weight percent	w%HS	*Misc.*
Quantitative estimate of drug likeness	qed_HS	*DFT (Pugar)*
Measured wavenumber of the free (non-hydrogen bonded) carbonyl (~1730 cm^{-1})	CO_free_W	*FTIR (Pugar)*
Urethane/Urea Classification	Ui	*FTIR (Pugar)*
Expected prepolymer degree of polymerization	PP_DP	*Step-growth kinetics (Pugar)*
Polyol melting point	SS_Tm	*DSC (Pugar)*
Difference in maximum partial charge of HS unit and maximum partial charge of SS unit for a sSS-TPU	MPC_HS-MPC_SS	*DFT (Pugar)*
Expected number of covalent backbone bonds per prepolymer	Avg Total_NumBonds_PP	*Step-growth kinetics (Pugar)*
Specific heat capacity at constant volume of polyol repeat unit	C (Cal/Mol/K)	*DFT*
Rotational contribution to specific heat capacity of polyol repeat unit	C,r	*DFT*
Translational contribution to specific heat capacity of polyol repeat unit	C,tr	*DFT*
Vibrational contribution to specific heat capacity of polyol repeat unit	C,v	*DFT*
Polyol degree of freedom	DP	*Misc.*
Electronegativity of polyol repeat unit	EN	*DFT*
HOMO energy of polyol repeat unit	Ehomo	*DFT*
Electronic energy of polyol repeat unit	Electronic Energy (Eh)	*DFT*
LUMO energy of polyol repeat unit	Elumo	*DFT*
Thermal energy of polyol repeat unit	Eth (Kcal/mol)	*DFT*
Rotational contribution to thermal energy of polyol repeat unit	Eth,r	*DFT*

Translational contribution to thermal energy of polyol repeat unit	Eth,tr	*DFT*
Vibrational contribution to thermal energy of polyol repeat unit	Eth,v	*DFT*
Fedor group contribution estimate of Flory-Huggins solubility parameter of polyol repeat unit	Fedor	*Flory-Huggins*
Difference between Fedor group contribution estimate of Flory-Huggins solubility parameter of polyol repeat unit and Stefanis group contribution estimate of hard segment (MDI + BDO) solubility parameter	Fedor_to_HS	*Flory-Huggins*
Difference between Fedor group contribution estimate of Flory-Huggins solubility parameter of polyol repeat unit and Stefanis group contribution estimate of MDI solubility parameter	Fedor_to_iso	*Flory-Huggins*
Number of hydrogen bond acceptors in polyol repeat unit	HBA	*RDKit*
HOMO-LUMO gap of polyol repeat unit	HL_gap	*DFT*
Hoy group contribution estimate of Flory-Huggins solubility parameter of polyol repeat unit	Hoy	*Flory-Huggins*
Difference between Hoy group contribution estimate of Flory-Huggins solubility parameter of polyol repeat unit and Stefanis group contribution estimate of MDI solubility parameter	Hoy_to_HS	*Flory-Huggins*
Difference between Hoy group contribution estimate of Flory-Huggins solubility parameter of polyol repeat unit and Stefanis group contribution estimate of MDI solubility parameter	Hoy_to_iso	*Flory-Huggins*
Number of heteroatoms in polyol repeat unit	NumHetero	*RDKit*
Number of rotatable bonds in polyol repeat unit	NumRotBonds	*RDKit*
Thermal entropy of polyol repeat unit	Sth (Cal/Mol/K)	*DFT*
Rotational contribution to thermal entropy of polyol repeat unit	Sth,r	*DFT*
Translational contribution to thermal entropy of polyol repeat unit	Sth,tr	*DFT*

Vibrational contribution to thermal entropy of polyol repeat unit	Sth,v	*DFT*
Topological Polar Surface Area of polyol repeat unit	TSPA	*RDKit*
Glass transition temperature of polyol	Tg	*DSC*
Melting Point of polyol	Tm	*DSC*
Dipole moment of polyol repeat unit	dipole moment (Debye)	*DFT*
Estimated reactivity of frontier orbitals of polyol repeat unit	frontier reactivity	*DFT*
Estimated chemical hardness of polyol repeat unit	hardness	*DFT*
octanol-water partition coefficient of polyol repeat unit	logP	*RDKit*
Polarizability of polyol repeat unit	polarizability (a.u.)	*DFT*